Available online at www.sciencedirect.com
ScienceDirect
Proceedings of the Combustion Institute 31 (2007) 3235–3242
Proceedings of the Combustion Institute
www.elsevier.com/locate/proci

Combustion in meso-scale vortex chambers

Ming-hsun Wu *, Yanxing Wang, Vigor Yang, Richard A. Yetter

Department of Mechanical and Nuclear Engineering, The Pennsylvania State University, 111 Research Building East, Bigler Rd., University Park, PA 16802, USA

Abstract

Vortex flows were utilized as a means to stabilize gaseous flames in meso-/micro-scale non-premixed combustors for use in small-scale power and propulsion systems. Scaling studies were performed with a series of combustors ranging in size from ~10.6 to 124 mm^3 (i.e., combustor diameters of 2.4–6.4 mm). Three-dimensional modeling of reacting flows was also conducted to explore flame stabilization mechanism and flow evolution in the chamber. Combustor performance was evaluated by analyzing the stability limit and chemical efficiency. Both hydrogen and hydrocarbons (methane and propane) have been studied with the chemical energy varying from 25 to 174 W. For the largest combustion volume, hydrogen and hydrocarbons burned efficiently in air. However, for smaller volumes, oxygen enrichment in air was required to stabilize hydrocarbon flames. Flame stabilization was achieved by a large, relatively quiescent, hot core flow that was formed by the flow recirculation at the head- and tail-ends of the combustor. The stability limits for hydrogen/air mixtures, in terms of the overall equivalence ratio, were found to be ~0.25 on the lean-side and in the range of 3–6 on the rich-side. The corresponding chemical efficiency exceeded 97%. For propane/air combustion, the stability limits ranged from ~0.25 to 2 for the 124 mm^3 combustor. Methane was the most difficult fuel to stabilize the flame and required oxygen-enriched air containing 40% O_2 and 60% N_2 by volume to operate in the 10.6 mm^3 combustor with a chemical efficiency of more than 85%.

Keywords: Vortex combustion; Meso-/micro-scale combustion

1. Introduction

Meso- and micro-scale combustion has been considered as a potential solution for many small-volume, energy demanding systems, such as power supplies for portable devices [1–4] and propulsion units for small spacecraft [5–7]. With the large energy densities of hydrocarbon fuels (~50 MJ/kg), combustion-based micro power devices remain surpassingly competitive with contemporary lithium batteries (~0.6 MJ/kg), even if the overall efficiency is as low as 10% [8].

As combustion volumes are reduced in size, issues of residence time, fluid mixing, thermal management, and wall quenching of gas-phase reactions become increasingly more important. The flow residence time in a small-scale combustor may become less than the chemical time for a premixed combustion system, or less than the combined mixing and chemical times for a non-premixed system, thus rendering complete combustion in the chamber a serious challenge [8]. The increased surface-to-volume ratio of a small combustor not only makes the heat generated from the combustion process hard to keep pace with the heat loss to the wall, but also enhances the possibility of radical termination by wall reactions. Such radical termination on the wall is

* Corresponding author. Fax: +1 814 865 3389.
E-mail address: minghswu@psu.edu (M. Wu).

1540-7489/$ - see front matter
doi:10.1016/j.proci.2006.08.114

chain breaking, and consequently prevents the radical growth essential for the branching and propagation of gas-phase reactions. On the other hand, the increased specific area of a miniaturized combustor makes surface-induced catalytic reactions [9–12] an attractive alternative. For small-scale combustors, extinction of confined flames often occurs as the portion of heat lost to the combustor body increases and less enthalpy is preserved in the combustion products. The resultant lower combustion temperature retards chemical reactions. To overcome this difficulty, the concept of "excess enthalpy" [12–15] has recently been introduced to extend the quenching limit of combustion in small combustors. The idea lies in redirection of hot burnt gases to preheat cold reactants without mass exchange, such that stable combustion can be sustained under conditions that would normally lead to flame extinction without recirculation. The catalytic and "excess enthalpy" designs, however, suffer from catalyst degradation and system complexity, respectively.

In the present work, vortex flows as a means to stabilize non-premixed gaseous flames in miniaturized combustors are investigated. A series of meso-scale combustors with volume as small as 10.6 mm^3 were fabricated and characterized with both hydrogen and hydrocarbon fuels (methane and propane). The system is based on the concept of asymmetric whirl combustion [16], which has demonstrated unusual stability characteristics for macro-scale combustors at very lean conditions. Experimental scaling analyses are also performed. In addition, a detailed numerical study of the three-dimensional flow fields is carried out to explore the flame stabilization mechanism. Results further verify the favorable temperature distribution and flow pattern of the asymmetric whirl combustion concept at meso scales.

2. Combustor configuration and experimental methods

Figure 1 shows the general configuration of a vortex combustor. Fuel is injected perpendicular to the tangentially injected oxidizer. The combustion products exit tangentially from the opposite end of the combustor. Intense mixing of fuel and oxidizer occurs at the inlets because of the direct impingement of the two streams. Such an injection scheme also avoids the potential hazard (e.g., flash-back) and system complexity associated with premixed systems. Compared with other swirl combustion concepts, which have also demonstrated their effectiveness in stabilizing flames in small volumes, vortex combustors developed in the present work have a much higher swirl number [17]. Moreover, the whirl flames should have a relatively stagnant center, whereas swirl flames are characterized by a vigorously burning central

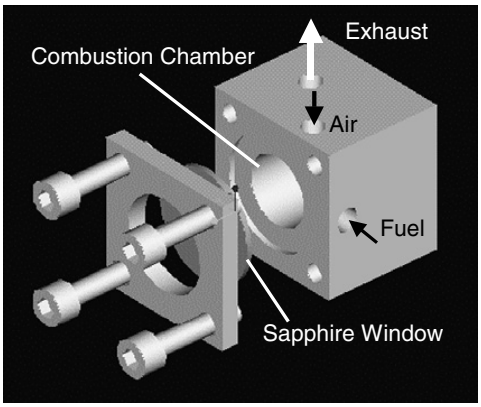

Fig. 1. Three-dimensional view of meso-scale combustor.

recirculation zone arising from the vortex breakdown of the swirling flow.

As the reacting flow rotates downstream towards the exit, the centrifugal force drives the fresh reactants to the wall, and the lighter hot flow remains in the core. The resultant flow structure and temperature stratification give rise to a lower temperature regime near the wall, and thus protect the chamber from reaching a high temperature. Note that the flame temperatures of both hydrogen and hydrocarbon combustion with air may far exceed the melting point of the combustor material, which is ~1700 K for Inconel.

A series of five millimeter-scale vortex combustors made of Inconel were fabricated using the electro-discharge machining (EDM) technique, as shown in Fig. 2. The combustion volume ranged from 10.6 to 107.8 mm^3. The diameters of the injection and exhaust ports were scaled with the combustor diameter. The chamber diameter-to-length ratio was near unity for all the combustors. For comparison, a combustor similarly scaled, but with a volume of 124 mm^3, was made of stainless steel using conventional machining.

In experiments, the reactants were ignited by either a glow (resistively heated platinum wire) or a spark igniter located at the center of the combustor head-end. The igniter was shut off immediately after a self-sustained flame was achieved. The sapphire optical window on the combustor was replaced by an end-port cap to house a thermocouple probe when conducting internal

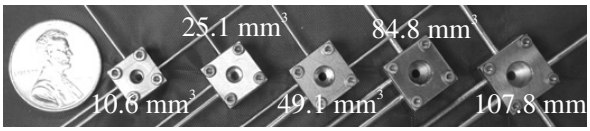

Fig. 2. Meso-scale vortex-stabilized combustors with volumes from left to right of 10.6, 25.1, 49.1, 84.8, and 107.8 mm^3, respectively. The corresponding diameters were 2.38, 3.18, 3.97, 4.76, and 5.16 mm.

temperature measurements. A water-cooled heat exchanger was installed for experiments using methane/oxygen-enriched air, in order to mitigate high temperature oxidation and corrosion of the exhaust tube. Such cooling also quenched any further reactions outside the combustion chamber to allow for a more accurate evaluation of the combustion efficiency. The reactants (purity > 99.5%) were regulated with commercial mass-flow controllers (Hastings, HFC-202) to the desired flow rates. The uncertainty in the flow rate measurements was ±2%. For experiments using oxygen-enriched air, oxygen and nitrogen were premixed at a desired ratio before being injected into the combustion chamber through the oxidizer port. Temperatures were measured with N-type thermocouples with a sheath diameter of 0.254 mm (0.01 in) (Omega, N-type). Combustor pressure was measured with a piezo-resistive pressure transducer (Omega, PX-176). In the present experiments, the operating pressure was maintained slightly above one atmosphere.

A Fourier transform infra-red analyzer (FT-IR) and micro gas chromatograph (GC) were utilized for emission measurements. The FT-IR spectrometer (ThermoNicolet, Nexus 670) had a cell path length of 10 cm and a volume of 100 cm^3. The resolution of the acquired absorption spectrum was 0.5 cm^{-1}. In the present experiments, the FT-IR analyzer was used to measure all carbon-containing gas species as well as water vapor. In order to obtain gas concentrations from molecules that lack permanent dipole moments, a gas chromatograph (Agilent, MicroGC 3000) was used to measure hydrogen, oxygen, and nitrogen. The GC was also employed to measure water vapor concentrations. The GC carrier gas was argon for both columns with their temperature set at 130 °C. The lower detection limit for GC measurements was 0.01% for the current configuration. The exhaust gas from the combustor was maintained above the water saturation vapor temperature in both the gas-transfer line and gas analyzers, thus, the samples were analyzed without drying.

3. Theoretical formulation and numerical methods

In parallel to experimental measurements, a numerical analysis was conducted to provide insights into the flow and flame evolution in the combustors. The formulation is based on the complete conservation equations for a multi-component chemically reactive system. Full account is taken of variable properties. Turbulence effects are neglected, since the Reynolds number (defined as UD/ν with U being the bulk axial velocity of the flow, D the chamber diameter, and ν the fluid kinetic viscosity) falls in the range of 50–500 for all the conditions studied. The one-step global kinetic schemes of Sekar and Mukunda [18] and Westbrook and Dryer [19] are employed for hydrogen/air and hydrocarbon/air systems, respectively. Boundary conditions at the chamber inlet and exit are treated by means of the method of characteristics. In addition, both adiabatic and isothermal conditions are considered at the wall, along with the enforcement of the no-slip conditions. A more detailed description of the formulation is given in Ref. [20]. The theoretical model is solved using a density-based, finite-volume approach. The numerical challenges associated with low-speed reacting flows are handled using a preconditioning scheme in conjunction with a pseudo-time iteration technique [21].

The spatial discretization employs a fourth-order and a second-order central difference scheme for convective and viscous terms, respectively. The pseudo-time derivatives are discretized using a four-step Runge–Kutta algorithm, with the real-time derivatives using a second-order backward difference scheme. All the calculations are conducted based on a Message Passing Interface (MPI) parallel computing architecture with a multi-block domain decomposition technique. The entire computation domain is decomposed into 37 sub-domains. The total grid points exceed one million, and the smallest grid size is 20 μm.

4. Results and discussion

Extensive experiments and numerical simulations have been conducted to characterize the combustor performance and to explore the detailed flow evolution and flame structures. In all the combustor volumes considered herein, stable flames were achieved over a wide range of flow rates and equivalence ratios for both hydrogen and hydrocarbon (including methane and propane) fuels, even in the smallest volume of 10.6 mm^3.

4.1. Flame structure and flow evolution

The flow development and flame structure are illustrated with numerical results for hydrogen/air combustion in the smallest combustor (10.6 mm^3). Figure 3 shows the 3-D stream traces of the reacting flow at $\phi = 0$ and $U_{in,air} = 100$ m/s. The wall temperature is fixed at 800 K, simulating the highest inner wall temperature measured in the combustor. Two kinds of flow recirculation can be identified. At the head-end of the combustor, the tangentially injected flow travels along the sidewall and recirculates azimuthally in the upstream regime before convecting downstream. The second recirculation zone is formed by a portion of the injected flow traveling directly downstream along the side-wall, turning backwards at the end plate, recirculating, and then exiting

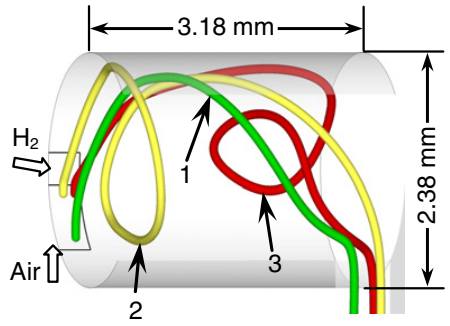

Fig. 3. Streaklines illustrating the flow evolution in H_2/air reacting flow at $\phi = 1.0$ and $U_{in,air} = 100$ m/s.

towards the exhaust. Consequently, the injected flow decomposes into three groups, a main flow and two minor branches. Figure 3 shows the streaklines originating from three different inlet locations. The main flow (path 1) rotates along the chamber-wall as it spirals towards the exit, and the two minor branches labeled as path 2 and 3 feed the upstream and down stream recirculation zones, respectively, as described above.

Regions of flow reversal are important to mixing and flame stabilization. To ensure efficient combustion, fast mixing and long residence times are required. The present combustor flow provides enhanced flame stabilization through generation of a relatively quiescent core flow. Figure 4 shows the 3-D structure of this flow reversal zone, which is created by the recirculating flows and is defined as the region in which the sign of the axial velocity is negative. In this relatively large zone, the velocity magnitude is much lower than that outside the zone. The reduction in velocity magnitude is critical in overcoming the high injection velocity and providing a region to anchor the flame.

Figure 5 shows the contours of the water mass fraction at cross-sections of $x = 0.4$ and 1.7 mm from the head-end and the 3-D iso-surface of water mass fraction at $Y_{H_2O} = 0.25$, which approximately locates the flame front. As a consequence of the threefold bifurcation of the injected flow at the entrance, the flame front decomposes into three branches, each propagating together

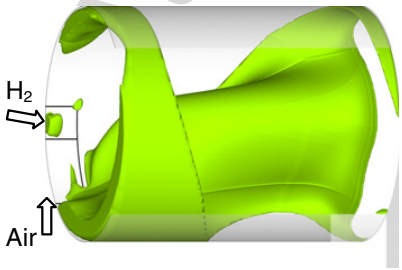

Fig. 4. 3-D structure of the flow reversal zone.

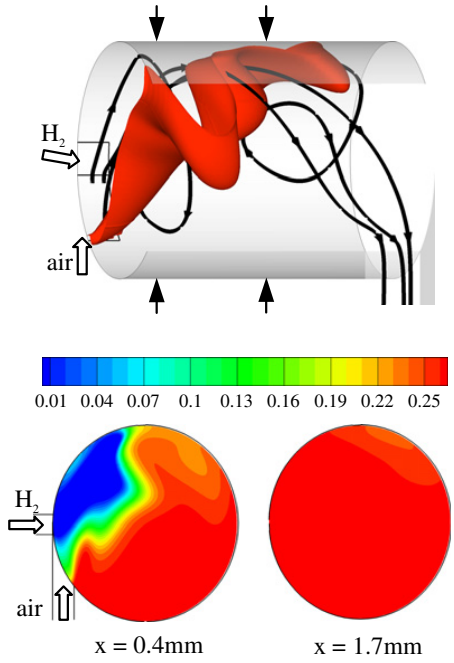

Fig. 5. Contours of water mass fraction at $x = 0.4$ and 1.7 mm and 3-D isosurface of water mass fraction at $Y_{H_2O} = 0.25$ for a combustor with diameter of 2.38 mm and operating on stoichiometric H_2/air. The vertical arrows in top figure locate the two cross-sections.

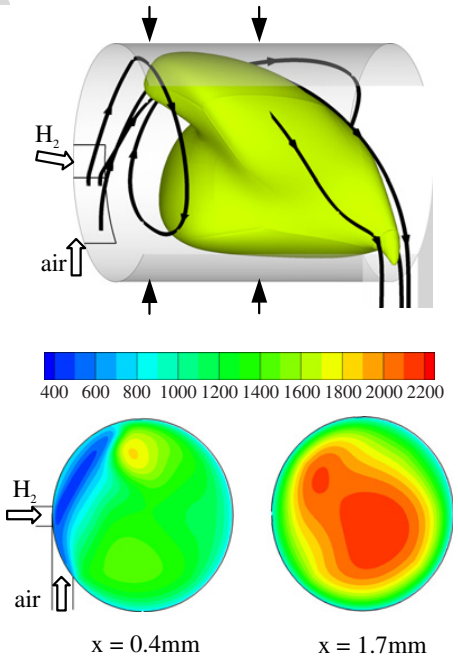

Fig. 6. Temperature contours at $x = 0.4$ and 1.7 mm and the isothermal surface at $T = 1800$ K for a combustor with diameter of 2.38 mm and operating on stoichiometric H_2/air.

with the corresponding flow along the side-wall to the exhaust.

Figure 6 shows the temperature fields of cross sections at $x = 0.4$ and 1.7 mm from the

head-end and the isothermal surface at $T = 1800$ K. As a result of heat loss from the solid wall, the average temperature in the combustor is lower than that of the adiabatic flame temperature. The temperature peak reaches ≈2400 K near the flame front. Evident from Fig. 6, the quiescent core flow not only provides a regime with reduced-velocity magnitude, but also serves as a high temperature source to preheat and ignite the reactants.

4.2. Characterization of hydrogen combustion

The flammability limits for hydrogen–air mixtures were obtained for three different combustion volumes of 10.6, 49.1, and 107.8 mm^3. Figure 7 shows the results for the 49.1 mm^3 combustor as a function of total mass flow rate. The overall equivalence ratio at the lean blow-off limit is around 0.25, whereas the rich limit varies from 3 to 6 depending on the reactant flow rate. The existence of the flame front was determined by temperature measurements with thermocouples located at the head-end center and exhaust port of the combustor. Results were confirmed independently by OH* emission measurements. The uncertainty of the measured blow-off limits are ±0.05 due to hysteresis effects in approaching the limits, the perturbation effects on the flame location by the presence of the thermocouple probe, and to the low intensity of OH* emission near extinction. It is worth noting that a piercing humming noise took place before the flame was blown-off.

Figure 8 shows the chemical efficiency of the three combustors. The total mass flow rate is 0.02 g/s for each combustor. The chemical efficiency for hydrogen/air combustion is defined as the ratio of the measured water vapor concentration to the summation of unburned hydrogen and water vapor concentrations in the product. Complete combustion was achieved in all three combustors when the overall equivalence ratio exceeds 0.4. The 49.1 mm^3 combustor gives a slightly larger operating space as the lean extinction limit is approached compared to the other two combustors. In these experiments, identical reactants flow rates were used for each combustor. Although the residence time was highest for the largest combustor, it also experienced the greatest heat loss. The residence time of the 10.6 mm^3 combustor was the smallest (~0.2 ms) and therefore least efficient in chemical conversion. Consequently, the 49.1 mm^3 was a compromise between the largest combustor with the greatest heat loss and the smallest combustor with the shortest residence time.

Figure 9 shows the combustion performance of the 107.8 and 49.1 mm^3 combustors operating at the same residence-time and power-density condition. The flow residence time, evaluated using the measured temperature, is ≈2 ms. The total mass

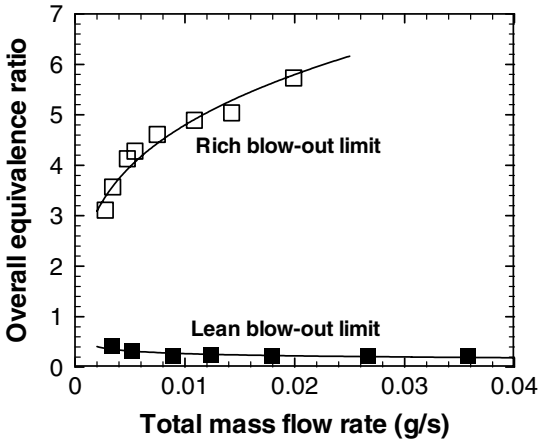

Fig. 7. Rich and lean stability limits of the 49.1 mm^3 combustor with H_2/air reactants.

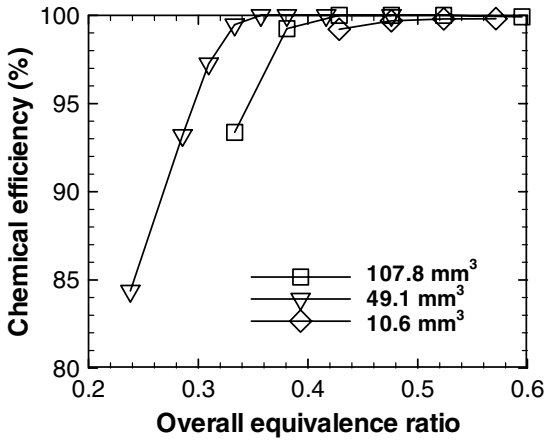

Fig. 8. Combustion efficiencies of H_2/air combustion in the three meso vortex combustors with a total mass flow rate = 0.02 g/s.

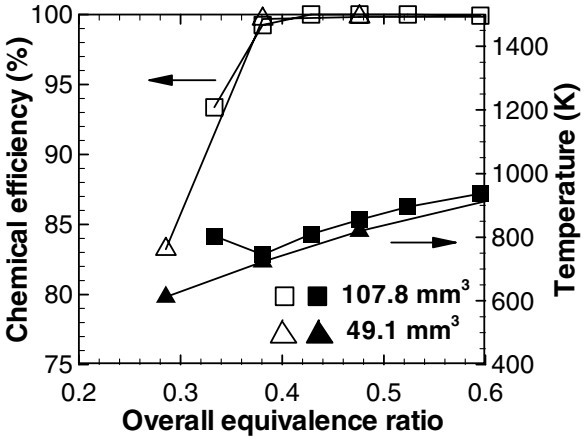

Fig. 9. Combustion efficiency and gas temperature for the 107.8 mm^3 combustor (total mass flow rate of 0.02 g/s) and for the 49.1 mm^3 combustor (total mass flow rate of 0.01 g/s) operating with H_2/air.

flow rates for the two combustors are 0.02 and 0.01 g/s, respectively. The two combustors have similar chemical efficiencies as well as the temperatures measured inside the combustor after scaling the chemical power input with the combustion chamber volume. The temperatures (not necessarily the maximum) were measured at the head-end on the center-line of the combustor approximately 0.3 diameter into the chamber. The delivered chemical power output under the conditions shown in Fig. 9 covers a range of 20–50 W.

Figure 10 shows the temperatures measured for a range of equivalence ratios from 0.2 to 0.6. The temperature for the 49.1 mm^3 combustor increases from 981 to 1319 K as the overall equivalence ratio increases from 0.3 to 0.5. Also included are the adiabatic flame temperatures and the outlet temperature of a perfectly stirred reactor (PSR) with chamber volume of 10.6 mm^3. The latter may provide a more reasonable benchmark for comparison since it takes into account the finite rate combustion kinetics as well as the thermal exchange of hot products with cold incoming reactants. Various definitions of thermal efficiency can be found in the literature [11,14] depending on the way in which the generated thermal energy is utilized. For example, for a heater and a thermal-photovoltaic power generator, the usable thermal energy is regarded as the portion that is transferred through the wall, whereas this is generally considered as heat "loss" for applications where high sensible energy is desired in the exhaust gas. In the present study, the thermal efficiency is defined as the ratio of the sensible energy in the combustion products to the total chemical power input. Such a definition is more suited for power plants or micro propulsion systems. It can be written mathematically in the following form:

$$\eta_t = \frac{\sum_k \dot{m}_k \bar{c}_{p,k}(T_c - T_i)}{\sum_i \dot{m}_i h_{c,i}} \times 100\%$$

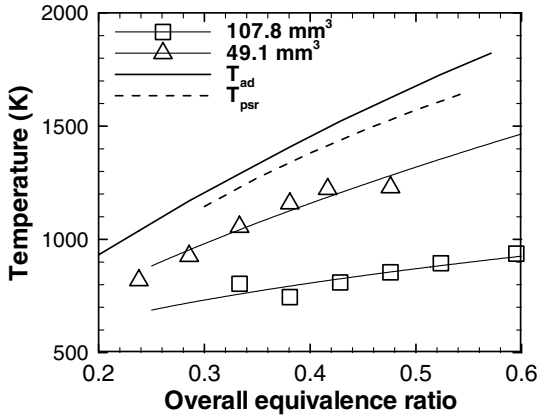

Fig. 10. Temperatures of H_2/air combustion measured in the 49.1 and 107.8 mm^3 combustion chambers.

where $\dot{m}_i$ and $h_{c,i}$ are the mass flow rate and heat of combustion of reactant species i, respectively, and is the mass flow rate of species k in the product. The constant-pressure heat capacity of species $k, \bar{c}_{p,k}$ is evaluated at the measured temperature, T_c, and the inlet temperature T_i is set at 298 K. The thermal efficiencies for the 49.1 mm^3 combustor were estimated to be 62 and 58% for $\phi = 0.3$ and 0.5. Their counterparts for the 107.8 mm^3 combustor were 40 and 32%, respectively. No temperature measurements were conducted in the 10.6 mm^3 volume due to the space constraints for installing thermocouples. As mentioned above, the measured temperatures were not necessarily the combustor average temperatures. Furthermore, attempts to control the thermal efficiency were not considered, and consequently, they were low while the chemical efficiencies were high.

4.3. Characterization of hydrocarbon combustion

Efforts were also applied to characterize the chemical efficiency and flame stability from hydrocarbon air systems. Figure 11a shows the front view of a propane/air flame with an overall equivalence ratio, ϕ, of 0.8. The chamber volume is 124 mm^3. The flame exhibits a luminous blue ring with a non-luminous core. The quenching distance is approximately 0.5 mm. The flame becomes bluish-green for fuel-rich mixtures. Under no conditions did the flame have a yellow emission characteristic of soot formation. Furthermore, carbon deposits were not observed on the inside of the chamber surface. The absence of soot formation suggests that the temperature inside the combustion zone was under 1650 K [22]. As inferred from the numerical calculations, the swirling flame structure observed herein results from the injection of fuel into the region of the highest kinetic energy of the whirling air flow, thereby producing rapid fuel-air mixing.

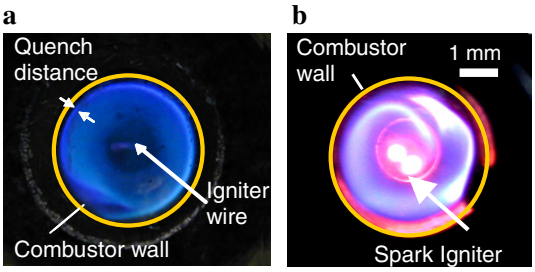

Fig. 11. Front views of the flame structure of (a) propane/air with an overall equivalence ratio of 0.8 in the 124 mm^3 combustor, (b) methane/oxygen- enriched air combustion in the 49.1 mm^3 combustor with an overall equivalence ratio of 0.3 (50% N_2 and 50% O_2 by volume in the oxidizer stream).

The resulting flow produces a central hot combustion product core and a spinning outer flame zone.

Figure 11b shows a typical flame structure of the methane/oxygen-enriched-air system in the 49.1 mm^3 combustor. The oxidizer contains 50% nitrogen and 50% oxygen, and the overall equivalence ratio is 0.3. A luminous blue swirling flame rotating along the chamber is clearly observed. Compared with the propane/air flame, the intense luminous flame zone results from more vigorous reactions of methane and oxygen-enriched air. The two bright spots in the center are caused by radiation from the spark igniter. Platinum glow-igniters were melted routinely, suggesting that the temperature at the combustor core might exceed the melting point of platinum, which is above 2000 K.

Combustion of hydrocarbon fuels in chamber volumes of tens of cubic millimeters is known to be challenging. The residence time required for efficient energy conversion is on the order of milliseconds, which is the same order as the characteristic chemical time for hydrocarbon/air combustion at room conditions. Methane and propane combustion with air was found more difficult as the combustor volumes were reduced. Self-sustained propane/air and methane/air flames were successfully stabilized in the 124 mm^3 combustor. However, stable methane combustion could only be achieved at atmospheric pressure in the smallest 10.6 mm^3 volume combustor by means of oxygen enrichment.

Figure 12 shows the effect of total mass flow rate on the lean and rich blow-off limits for the propane/air system in the 124 mm^3 combustor. The limits appear to increase with increasing flow rate. At a total mass flow rate of 0.02 g/s, the lean and rich blow-off limits occurred at equivalence ratios of ≈0.4 and 1.6, respectively. The corresponding flammability limits for well-mixed propane in air are 0.56 and 2.7, respectively. The difference of flammability between the present

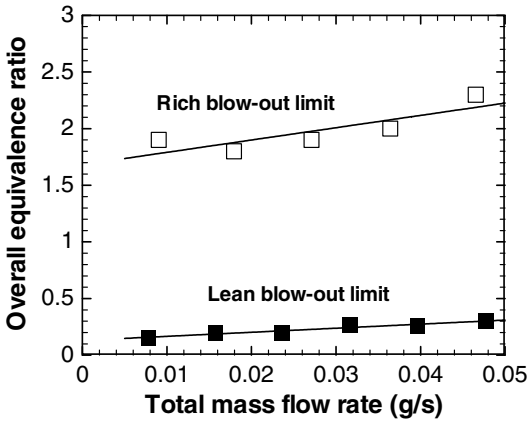

Fig. 12. Stability limits of propane/air combustion in the 124 mm^3 combustor.

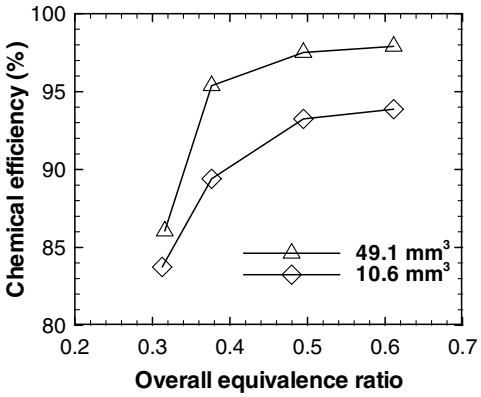

Fig. 13. Combustion efficiency of methane and oxygen-enriched air in the 49.1 and 10.6 mm^3 combustors.

combustor and a premixed system suggests that stratification remains in the mixture during combustion. The measured temperatures in the flow core region along the centerline are ≈1500 K for an equivalence ratio of 0.75.

In the present research, only exhaust gas composition of the vortex combustors fueled with methane were obtained. Measurements were conducted using the FT-IR analyzer to obtain absolute concentrations. Since no other carbon containing species except CO_2, CO, and unburned CH_4 were observed in the FT-IR spectra under fuel-lean conditions, the chemical efficiency of methane combustion was defined as the ratio of the measured concentration between carbon dioxide and all carbon-containing species. Figure 13 shows the chemical efficiencies of methane/air combustion with oxygen enrichment in the 10.6 and 49.1 mm^3 combustors. The oxidizer mixture contains 40% O_2 and 60% N_2, and the total mass flow rate remained constant at 0.02 g/s. As expected, efficiency is lower for a smaller volume due to the shorter flow residence time. The delivered chemical output from the 10.6 mm^3 combustor ranged from ≈25 to 174 W. The residence time for the flow rate evaluated at standard conditions was ≈0.6 ms. With stable combustion, the results of Fig. 13 show that good chemical efficiencies are attainable in the smallest combustors with hydrocarbons which were even higher in the larger combustors.

5. Conclusions

The concept of asymmetric injection and vortex combustion has been successfully implemented and demonstrated to stabilize flames in small volumes ranging from 10.6 to 124 mm^3. Both hydrogen and hydrocarbon (methane and propane) in air were treated. Methane was the most difficult to stabilize, but could be stabilized in all the combustors with enrichment of the air to an oxygen

level of 40% by volume. Chemical efficiencies were generally high exceeding 97% for hydrogen/air and 85% for methane/oxygen-enriched air. Numerical analysis indicated that flame stabilization was achieved by flow recirculation creating a nearly quiescent region of hot combustion products in the combustor core.

Acknowledgments

This work was supported by the Air Force Office of Scientific Research under Contract AFOSR F49620-01-1-0376. The authors gratefully acknowledge the support from Dr. Mitat Birkan, contract monitor, of the program.

References

[1] W.M. Yang, S.K. Chou, C. Shu, Z.W. Li, H. Xue, *Appl. Phys. Lett.* 81 (27) (2002) 5255–5257.
[2] D.C. Kyritsis, S. Roychoudhury, C.S. McEnally, L.D. Pfefferle, A. Gomez, *Exp. Thermal Fluid Sci.* 28 (7) (2004) 763–770.
[3] L.M. Matta, M. Nan, S.P. Davis, D.V. McAliister, B.T. Zinn, M.G. Allen, in: The 39th AIAA Aerospace Sciences Meeting and Exhibition, Reno, NV, USA, 2001.
[4] I.A. Waitz, G. Gauba, Y.S. Tzeng, *J. Fluids Eng. Trans. ASME* 120 (1) (1998) 109–117.
[5] R.A. Yetter, V. Yang, Z. Wang,Y. Wang, in: The 41st AIAA Aerospace Sciences Meeting and Exhibition, Reno, NV, USA, 2003.
[6] A.P. London, A.A. Ayon, A.H. Epstein, et al., *Sensors Actuators A* 92 (1–3) (2001) 351–357.
[7] C. Rossi, T. Do Conto, D. Esteve, B. Larangot, *Smart Mater. Struct.* 10 (6) (2001) 1156–1162.
[8] A.C. Fernandez-Pello, *Proc. Combust. Inst.* 29 (2003) 883–899.
[9] D.C. Kyritsis, B. Coriton, F. Faure, S. Roychoudhury, A. Gomez, *Combust. Flame* 139 (1–2) (2004) 77–89.
[10] K. Maruta, K. Takeda, J. Ahn, et al., *Proc. Combust. Inst.* 29 (2003) 957–963.
[11] C.M. Spadaccini, X. Zhang, C.P. Cadou, N. Miki, I.A. Waitz, *Sensors Actuators A* 103 (1-2) (2003) 219–224.
[12] J. Vican, B.F. Gajdeczko, F.L. Dryer, D.L. Milius, I.A. Aksay, R.A. Yetter, *Proc. Combust. Inst.* 29 (2003) 909–916.
[13] P.D. Ronney, *Combust. Flame* 135 (2003) 421–439.
[14] N.I. Kim, S. Kato, T. Kataoka, et al., *Combust. Flame* 141 (2005) 229–240.
[15] F.J. Weinberg, D.M. Rowe, G. Min, P.D. Ronney, *Proc. Combust. Inst.* 29 (2003) 941–947.
[16] R.A. Yetter, I. Glassman, H.C. Gabler, *Proc. Combust. Inst.* 28 (2000) 1265–1272.
[17] W.A. Sirignano, T.K. Pham, D. Dunn-Rankin, *Proc. Combust. Inst.* 29 (2002) 925–931.
[18] B. Sekar, H.S. Mukunda, *Proc. Combust. Inst.* 23 (1990) 707–713.
[19] C.K. Westbrook, F.L. Dryer, *Combust. Sci. Technol.* 27 (1-2) (1981) 31–43.
[20] Y. Wang, M.-H. Wu, R.A. Yetter, V. Yang, in: The 43rd AIAA Aerospace Sciences Meeting and Exhibition, Reno, NV, 2005.
[21] S.-Y. Hsieh, V. Yang, *Int. J. Comput. Fluid Dyn.* 8 (1997) 31–49.
[22] I. Glassman, *Combustion*, third ed., Academic Press, San Diego, USA, 1996.

Comments

Alessandro Gomez, Yale University, USA. As the combustor becomes smaller and smaller, the surface-to-volume ratio increases; as a result, the thermal efficiency ought to decrease. Your data seem to show an opposite trend. How do you explain your findings?

Reply. The results we show in Fig. 10 are the thermal efficiencies of the 49.1 and 107.8 mm^3 combustors under the same total mass flow rate, 0.02 g/s. As a result, although the smaller combustor has a larger surface-to-volume ratio, the flow residence time is shorter in the 49.1 mm^3 combustor. While the residence time is still sufficient for complete chemical reaction to occur even in the smaller combustor (Fig. 9), the longer residence time in the larger combustor means that there is a longer time for heat loss, which results in the lower thermal efficiency in the larger combustor.

•

Derek Dunn-Rankin, University of California, Irvine, USA. The images of the swirl combustor indicate a glowing residual "hot-spot" at the location of the igniter (glow wire or spark plug) even after the electrical ignition source is turned off. Similarly, model airplane engines use the local heat retained in a glow plug wire to ignite the fresh mixture. Does the glowing hot spot aid in combustion stability in your system and was a hot spot included in the numerical simulation?

Reply. The glowing spark electrodes could have an effect on flame stabilization, but we do not expect this effect to be significant. The convective heat transfer from flow over the 0.254 mm O.D. spark wires is unlikely to be larger than the direct mass and thermal exchange in the recirculation zones. A hot spot was not included in the numerical simulation.